NASA
Technical
Paper
2200

September 1983

Three-Dimensional Turbulent-Mixing-Length Modeling for Discrete-Hole Coolant Injection Into a Crossflow

Chi-Rong Wang and
S. Stephen Papell

NASA

25th Anniversary
1958-1983

NASA
Technical
Paper
2200

1983

Three-Dimensional Turbulent-Mixing-Length Modeling for Discrete-Hole Coolant Injection Into a Crossflow

Chi-Rong Wang and
S. Stephen Papell

Lewis Research Center
Cleveland, Ohio

National Aeronautics
and Space Administration

**Scientific and Technical
Information Branch**

Summary

Three-dimensional mixing length models were developed for the analysis of flow field a small distance (less than 10 coolant hole diameters) downstream of coolant injection through a discrete hole at a 30° angle into a crossflowing free stream. The experimental data, obtained with a hot wire sensor to probe the flow field, were used to determine the local mixing length. Mixing length models for the coolant exit region, separated flow region, and the reattachment flow region were inferred from the local mixing length distributions. To verify the mixing length modeling, conservation equations in a theoretical analysis were simplified and solved numerically, using the mixing length models to estimate the turbulence effects and to predict the velocity and temperature fields. With small injection rate and constant wall temperature, the numerical results of the crossflow streamwise velocity component and the surface heat-transfer rate were consistent with the hot-wire velocity measurements and with the results of the surface film cooling effectiveness study. With more detailed experiments, these mixing length models can be improved and used in theoretical analyses to study the effects of coolant temperature and turbulence on the discrete hole surface film cooling process.

Introduction

Coolant injection through discrete holes at an acute angle to the external flow is widely used for turbine blade surface cooling. The convective heat-transfer coefficient along the surface downstream of coolant injection is an important factor in determining film cooling effectiveness. Usually this heat-transfer coefficient is determined experimentally by measuring the local heat transfer rate; it is sometimes derived from the results of a two-dimensional boundary-layer flow analysis. Because of the complicated three-dimensional flow field associated with discrete-hole cooling, especially in the region near the coolant hole, two-dimensional boundary layer flow analysis is inadequate to predict the local heat transfer rate. A three-dimensional computational method to predict this surface heat transfer rate is therefore needed. The technique of modeling the turbulent effects due to the mixing between the coolant flow and the external crossflow has been a major factor in the success of current computational methods. Thus, the objective of the present study was to develop three-dimensional mixing length models for use in the analysis of the flow field a small distance (less than 10 coolant hole diameters) downstream of a coolant hole.

Recently, many theoretical analyses and experiments have been performed to study the turbulent mixing of discrete-hole film cooling. Experiments (refs. 1 to 3) indicate that the coolant mixing layer turns toward the wall surface near the coolant exit and that the flow separates from and reattaches to the wall surface a small distance downstream of the coolant hole. Theories for predicting the flow process appear in references 4 to 6. The numerical technique applied in references 5 and 6 to predict the surface film cooling effectiveness was described in reference 7. An anisotropy coefficient was used in reference 6 to approximate the normal and lateral turbulent effects. Turbulent mixing length models, with linear mixing length distributions between pivot points, were used in reference 8 to compute numerically the flow properties immediately downstream of a two-dimensional tangential slot injection flow process. The present authors intend to develop similar types of mixing length model for the three-dimensional flow field considered here.

In this paper three-dimensional mixing length models are presented for the coolant exit region, the separated flow region, and the reattachment flow region. These models were derived from the calculated local mixing length distributions obtained from the measured turbulence intensities. The resulting mixing length models are then used in a simplified theoretical analysis of the flow field to assess the effectiveness of these models. For this analysis, the governing conservation equations are solved numerically using an existing finite-difference scheme. The computed velocity and heat-transfer distributions are compared with the experimental results.

Symbols

C_p constant pressure specific heat
D coolant tube diameter
E_b anemometer dc voltage
E_{b0} anemometer dc voltage at zero velocity
e_b rms value of anemometer ac voltage
F_{12} empirical constant, $=0.59$
K heat conductivity
k turbulent kinetic energy
l local turbulent mixing length
l_δ mixing length at $u \geq \delta$
l_0 mixing length at $y=0$
l_1 mixing length at pivot point 1
l_2 mixing length at pivot point 2
P local generation rate of ϵ
R_F crossflow free-stream Reynolds number per meter
St Stanton number, equation (15)
St_0 initial Stanton number
T local mean temperature

T_F free-stream mean temperature
T_J coolant mean temperature
T_w wall surface temperature
t fluctuating temperature
$\overline{U}$ local mean velocity along x direction
u fluctuating velocity in x direction
$\overline{U_F}$ crossflow free-stream mean velocity
$\overline{U_J}$ coolant mean velocity
$\overline{V}$ local mean velocity along y direction
v fluctuating velocity in y direction
$\overline{W}$ local mean velocity in z direction
w fluctuating velocity in z direction
x longitudinal coordinate
x_1 longitudinal location where $x=D$
x_2 longitudinal location where $x=2D$
x_s longitudinal reattachment location
y normal coordinate
y_1 y coordinate at pivot point 1
y_2 y coordinate at pivot point 2
y_δ y coordinate at $y=\delta$
z lateral coordinate
z_c lateral coordinate at edge of coolant hole
z_1 U_j = constant for $z \leq z_1$
z_2 l unchanged for $z \geq z_2$
α_1 empirical constant, $=0.94$
α_2 empirical constant, $=0.26$
δ velocity boundary layer thickness
ϵ turbulent kinetic energy dissipation rate
θ coolant injection angle
λ coolant injection mass flow rate, $=\rho_J\overline{U_J}/\rho_F\overline{U_F}$
μ absolute viscosity
ρ local density
ρ_F crossflow free-stream density
ρ_J coolant density

Theoretical Analysis of the Flow Field

The flow field of interest in the present study is a small region within 10 x/D of coolant injection. A schematic of this flow region is shown in figure 1. The profiles of the mean velocity, mean temperature, and turbulent mixing length of the incoming crossflow are assumed to be two dimensional. The coolant is injected into the crossflow through a circular tube at a 30° angle to the wall.

The mathematical model for an analysis of this type of discrete-hole cooling process is given in detail in reference 5. The steady, three-dimensional turbulent flow field is described with continuity, momentum, and energy equations. That analysis is also used here. The set of the governing equations, the boundary conditions, and the closure assumptions, which solve analytically the velocity and the temperature fields, are given in the appendix. The x-direction gradients of the stresses and enthalpy flux and all the pressure gradient terms were neglected in the conservation equations of this study. This allows the effectiveness of the three-dimensional mixing length models to be assessed in a simple manner.

The closure assumptions (eqs. (A7) to (A14)) require further information on the mixing length distribution before they can be used in the conservation equations. Thus, wind tunnel experiments with coolant air injection were performed to establish the turbulent mixing length models.

Experiment and Data Analysis

Details of the experimental apparatus were previously described in reference 9. The principal components included the tunnel, the test section plenum assembly, and a Hilsch tube for coolant air supply. The tunnel itself was made of clear plastic sections with a flow area section of 15 by 38 cm. The coolant injection hole (1.27 cm diam) was located in the lower wall of the test section. The boundary layer thickness was 1.65 cm ahead of the coolant hole with a crossflow velocity $\overline{U_F}$ of 22.9 m/sec. The mean velocity $\overline{U}$ and the turbulence intensity, $(\overline{u^2})^{1/2}/\overline{U}$ along the crossflow direction were measured with a single-sensor tungsten hot-wire probe. The axis of the sensor was parallel to the wall surface and perpendicular to the crossflow streamwise direction. To

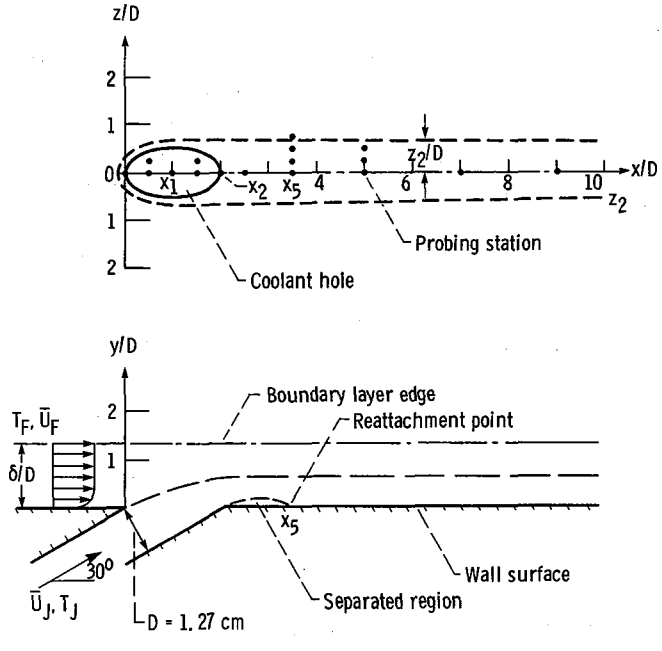

Figure 1. - Schematic of flow field.

take the measurements at locations across the boundary layer, the probe was traversed normally from the wall surface towards the external crossflow.

Measurements

The bridge dc voltages and the rms of the ac voltage were measured at $x/D=0$, 0.5, 1.0, 1.5, 2.0, 2.5, 3.5, 5.0, 7.0, and 9.0 within the symmetric plane ($z/D=0$). Similar measurements were taken at selected lateral locations, $z/D=0.25$, 0.50, and 0.75, at $x/D=3.5$ and 5.0 (fig. 1). These data were collected at injection rates λ of 0.22 and 0.37.

Mixing Length Computation

The local turbulence intensity $(\overline{u^2})^{1/2}/\overline{U}$ was computed using the following equation:

$$\frac{\overline{u^2}}{\overline{U}} = \frac{4E_b e_b}{(E_b^2 - E_{b0}^2)} \tag{1}$$

which has derived from King's law. This measured turbulence intensity was used to compute the local mixing length with the modified Reynolds stress transport equation developed by Hanjalic and Launder (ref. 10):

$$\overline{u^2} = \frac{\alpha_1}{\alpha_2} l^2 \left[\left(\frac{\partial \overline{U}}{\partial y} \right)^2 + \left(\frac{\partial \overline{U}}{\partial z} \right)^2 \right] \tag{2}$$

where α_1 and α_2 were empirical constants (see appendix). The normal and lateral gradients of the $\overline{U}$ velocity component were derived from the velocity profile measurements.

Results of the Experimental Mixing Length

Examples of the mixing length distributions, as computed from equations (1) and (2), are given in figures 2 to 7. Figures 2 and 3 show the distributions over the coolant hole exit for the two injection rates, and figure 4 shows the distributions downstream of the coolant hole. Lateral variations in the mixing length distributions are shown in figures 5 to 7 for different injection rates and longitudinal locations. For the present range of injection rates ($\lambda<0.4$), these experimental mixing length distributions could be approximated with segmented linear functions of y with pivot points y_1, y_2, and y_δ.

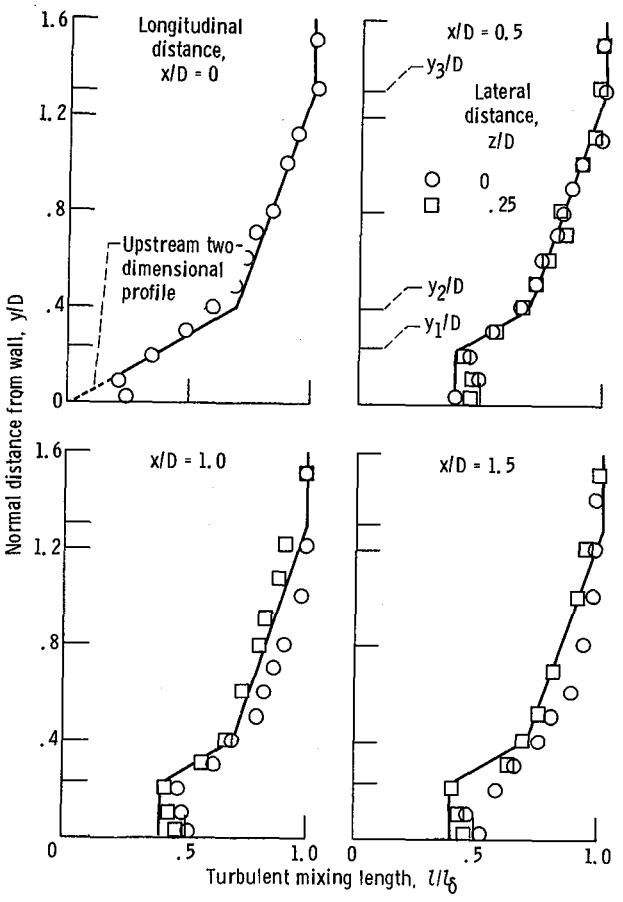

Figure 2. - Mixing length distributions over coolant exit region. Coolant injection mass flow rate, 0.22.

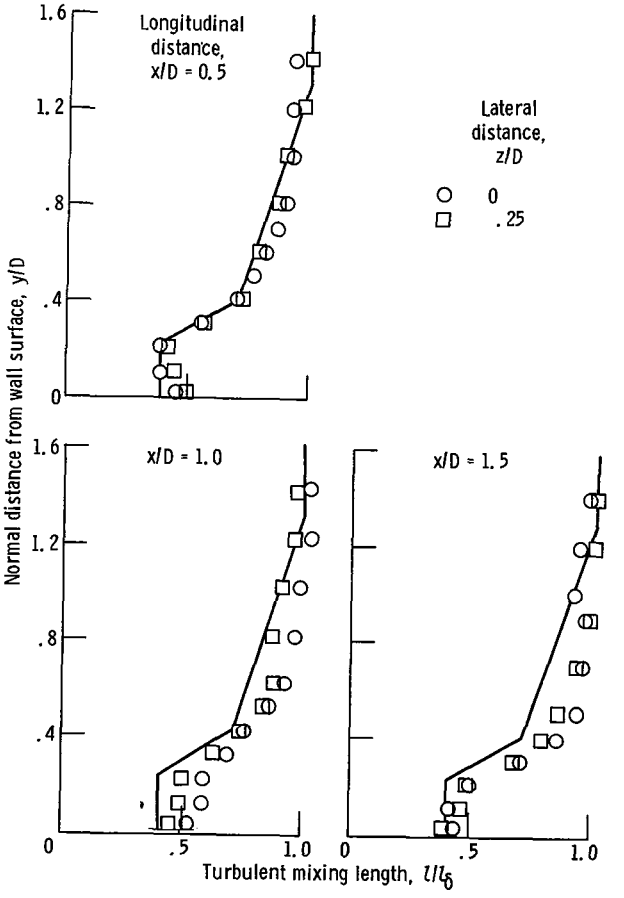

Figure 3. - Variations of mixing length over coolant exit. Coolant injection mass flow rate, 0.37.

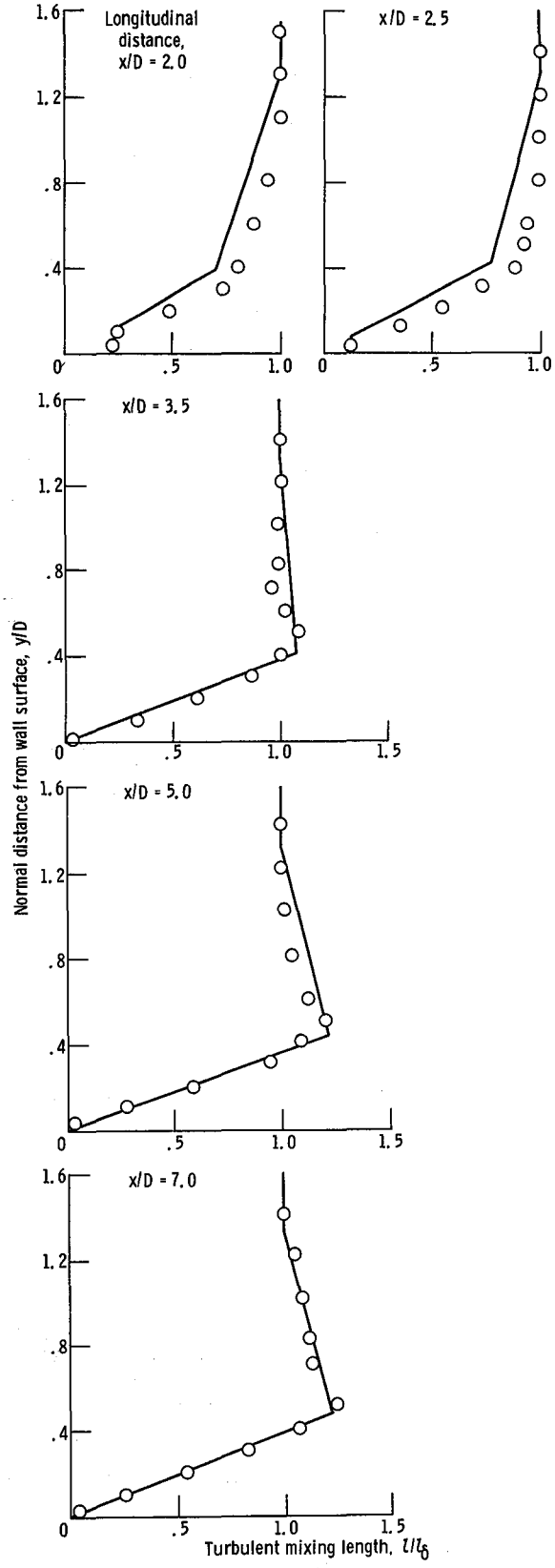

Figure 4. - Mixing length distributions within plane of symmetry at z/D = 0. Coolant injection mass flow rate, 0.22.

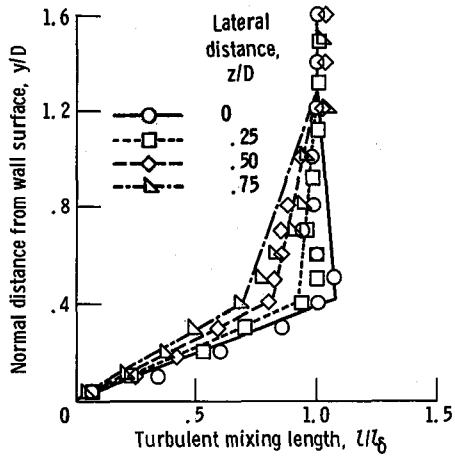

Figure 5. - Lateral variations of mixing length at x/D = 3.5. Coolant injection mass flow rate, 0.22.

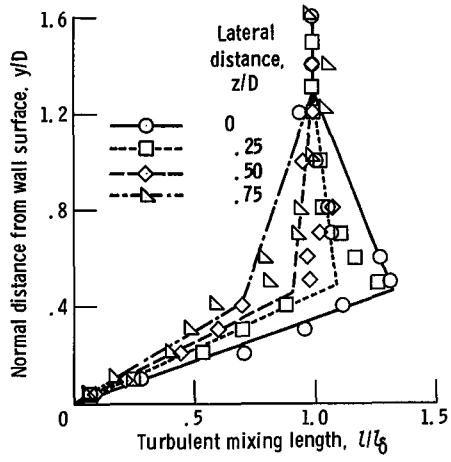

Figure 6. - Lateral variations of mixing length at x/D = 3.5. Coolant injection mass flow rate, 0.37.

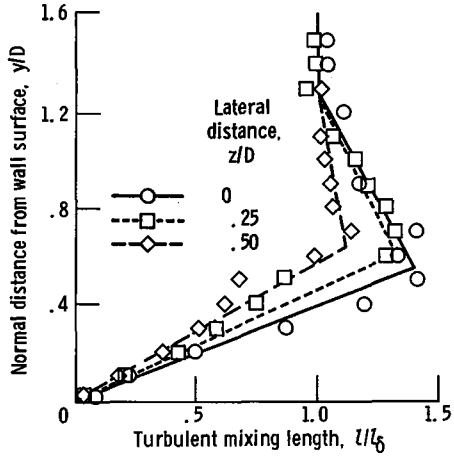

Figure 7. - Lateral turbulent mixing length distributions at x/D = 5.0. Coolant injection mass flow rate, 0.37.

However, the basic shape of the mixing length distribution changes as a function of longitudinal and lateral position. Coolant injection ($\lambda \leq 0.4$) did not disturb the mixing length distribution near the boundary-layer edge, and the edge of the boundary layer was taken as the outer pivot point. For $y \geq \delta$ the crossflow free-stream mixing length was 0.26 cm, with the following conditions: $\overline{U}_F = 22.9$ m/sec, $T_F = 300$ K, and $R_F = 1.54 \times 10^6$.

The mixing length distribution was different from that of the upstream undisturbed boundary layer only in a region close to the coolant exit where constant mixing length was found. (See figs. 2 to 4.) The local mixing length in the boundary layer increased, especially within the symmetric plane, after the coolant exit (fig. 4). The maximum turbulent mixing length l_2 and the near-surface ($y/D = 0.04$) mixing length l_1 within the $z/D = 0$ plane are shown in figure 8. A large variation in mixing length occurred in a region ($x/D \leq 5$ for $\lambda = 0.37$) immediately downstream of the coolant injection. After this region zero mixing length near the wall surface l_1 and constant l_2 ($\geq l_\delta$) were found at the x/D locations within the limit of the present study. The lateral variation of the maximum mixing length l_2 is shown in figure 9. The experimental data are well represented by straight lines.

Slope $\partial l/\partial y$, where $0 \leq y \leq y_2$ at $x/D = 3.5$ and 5, was also determined from the experimental results and plotted (fig. 10). The effect of the coolant injection rate on $\partial l/\partial y$ may be neglected for the cases considered.

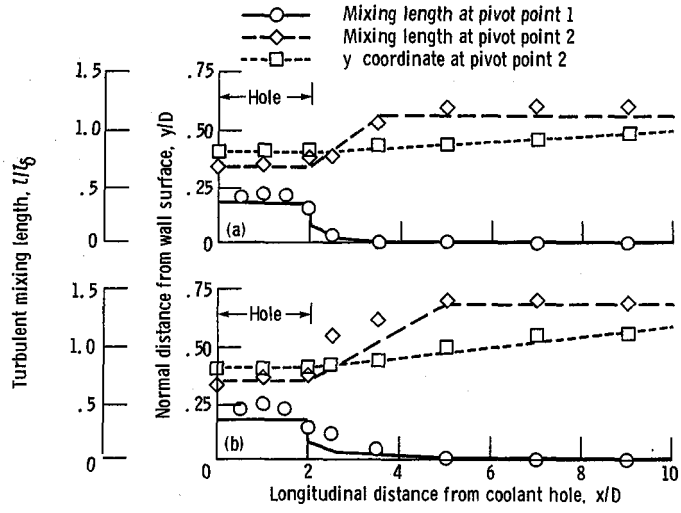

(a) Coolant injection mass flow rate, 0.22.
(b) Coolant injection mass flow rate, 0.37.

Figure 8. - Experimental results of l_1, l_2 and y_2 within $z = 0$ plane.

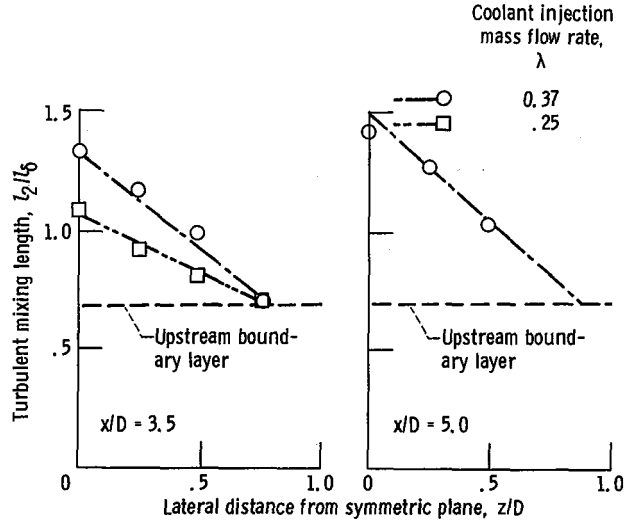

Figure 9. - Lateral variations of mixing length at pivot point 2.

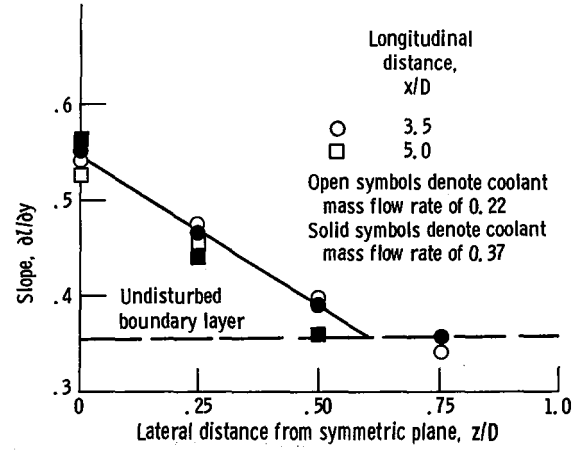

Figure 10. - Lateral variation of slope ($\partial l/\partial y$); $0 \leq y \leq y_2$.

Three-Dimensional Mixing Length Modeling

From the preceding experimental results, the present authors categorized the local turbulent mixing length distributions within the flow field of interest into three models corresponding to the coolant exit region, the separated flow region, and the reattachment flow region. The present models are derived from the comparisons of the normal direction mixing length distribution with the mixing length profile within the upstream boundary layer. This mixing length profile is approximated by three linear functions of y with pivot points, $y_2 = 0.3\,\delta$, $l_2 = 0.18$ cm and $y = \delta$, $l_\delta = 0.26$ cm (fig. 11(a)). Because of the insufficient data in the lateral direction, some assumptions are made in the following modeling.

Coolant Exit Region

For the coolant exit region (fig. 11(a)) turbulent mixing length immediately over the coolant hole exit must be prescribed for this modeling (it was derived from the experimental data in the present study). The turbulent mixing length profile can then be determined as it is

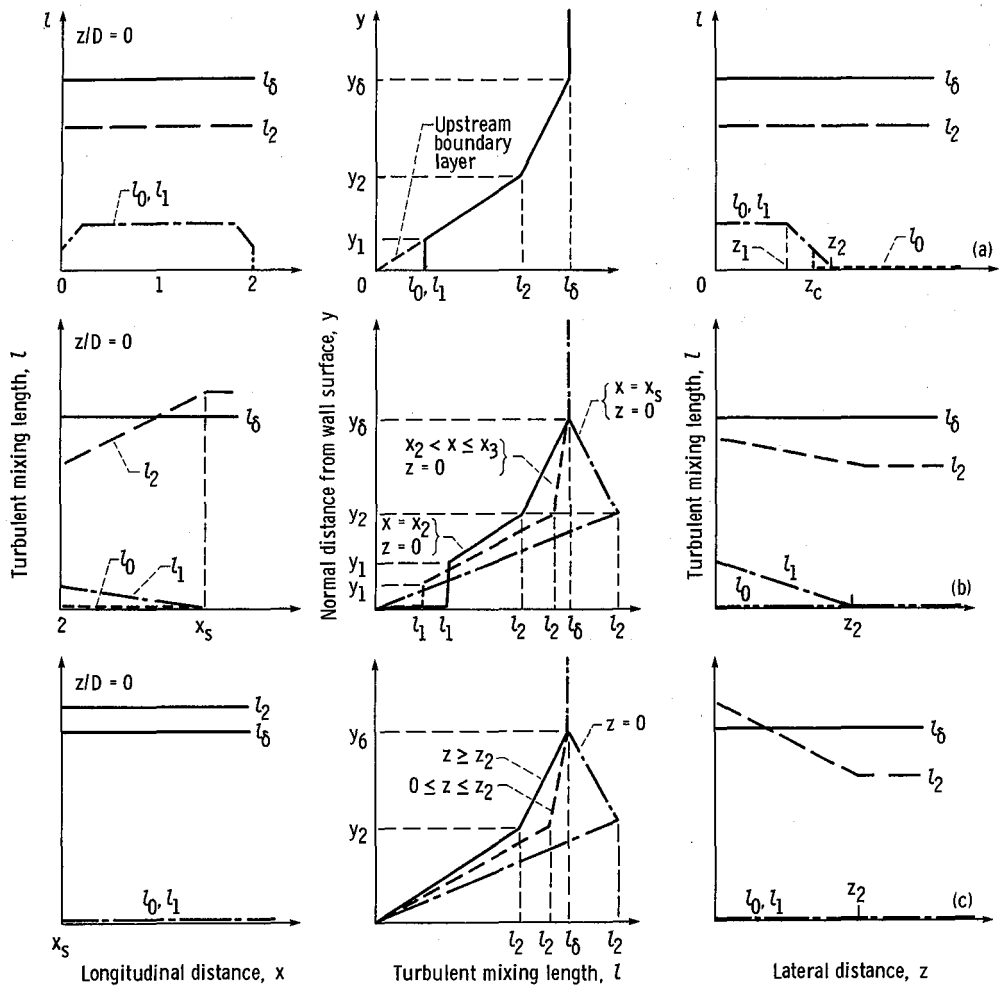

(a) Coolant exit region.
(b) Separated flow region.
(c) Reattachment flow region.

Figure 11. - Turbulent mixing length models.

presented in the figure. Mixing lengths l_0 and l_1 were assumed to be constant along the z direction for $0 \le z \le z_1$ and then to decrease linearly after z became greater than z_1. The mixing length l_0 is set to zero at the wall surface for $z \ge z_c$; l_2 and l_δ are the same as those of the upstream profile.

Separated Flow Region

The separated flow region (fig. 11(b)), is characterized by a large mixing length l_1 near the surface and increasing l_2 at different x/D. A linear variation in $\partial l/\partial y$ for $y_1 \le y \le y_2$ as a function of x along the symmetric plane and a constant l_1 for $0 < y \le y_1$ are assumed. Mixing length $l_0 = 0$ is also imposed at $y = 0$.

Along the lateral direction l_1 changes linearly from the centerline value to zero at z_2. Linear variation in $\partial l/\partial y$ for $y_1 \le y \le y_2$ as a function of z is also assumed in $0 \le z \le z_2$. The mixing length profile retains the undisturbed boundary layer profile for $z \ge z_2$.

Reattachment Flow Region

For the reattachment region (fig. 11(c)) both l_0 and l_1 are zero. Thus, within the plane of symmetry, the mixing length distribution is defined by l_2 and y_2 once they are given. A linear variation in $\partial l/\partial y$ (between the pivot points $y = 0$ and $y = y_2$) as a function of z is assumed for $0 \le z \le z_2$ to define the lateral mixing length distribution. The undisturbed boundary layer mixing length profile exists in $z \ge z_2$.

In the previous models assumptions have been made at $z = z_1$ or z_2, and the properties l_1, l_2, and y_2 are also considered to be given at the pivot points. To completely define the mixing length models requires more detailed experimental results to establish empirical relations for these parameters. For the following computational verification of the present proposed models, linear approximations over the present experimental $y_2(x)$, $l_1(x)$, and $l_2(x)$ in the symmetric plane are used. The assumptions for the determination of z_1 and z_2 will be

described, with the boundary condition assumptions, in the following sections.

Numerical Method and Assumptions

The numerical procedures described in reference 11 were used to write a set of finite difference equations corresponding to the governing conservation equations presented in the appendix. The finite difference equations were then solved numerically with a noniterative marching technique in the x direction and the standard tri-diagonal matrix algorithm to obtain the velocity and temperature distributions.

The boundary conditions of the velocity and turbulent mixing length distributions at the coolant exit ($y=0$) are shown in figure 12. Constant velocity components ($\overline{U}$, $\overline{V}$) within the ellipse (major axis = 1.6 D, minor axis = 0.8 D) enclosed by z_1 and linear $\overline{U}$ variation along the z direction for $z_1 \leq z \leq z_c$ are assumed. Assumptions of these properties along the x-direction in the $z=0$ plane are also given in this figure. An upstream disturbance distance of 0.2 D along the $z=0$ symmetric plane, with the undisturbed two-dimensional mean velocity and temperature profiles in the y-z plane at this location ($x=-0.2\ D$), is also assumed. These boundary conditions are not changed with different rates of coolant injection.

An ellipse centered at $x=x_1$, $z=0$ is assumed for z_2 for $x \leq x_1$. Constant z_2 from x_1 to x_s and the experimental results (fig. 5) are then used to determine z_2 for $x \geq x_s$. Constant y_2 in the $z \leq z_2$ is also assumed, and a step change in y_2 occurs at $z=z_2$. The size of the computational domain in the y-z plane was 1.5 D by 2 D and the grid point dimension was 35 by 61 for the present computations. However, a variable Δx step size (300 steps for $\lambda=0.22$ and 500 steps for $\lambda=0.37$) with smaller Δx over the coolant exit region was used for $x/D \leq 10$. To reduce the numerical diffusion and to avoid the use of fine grids near the wall surface, a local maximum value of $\partial\overline{U}/\partial z = 500$, and $\partial\overline{U}/\partial y$ (fig. 13), through linear interpolation between the value in $z=0$ plane and those from the power law profile at z_2, were imposed in the numerical process. The $\partial\overline{U}/\partial y$ at the wall surface ($y=0$) was determined from the universal velocity profile assuming a sublayer existed there.

To solve the kinetic energy dissipation rate equation, the turbulent kinetic energy at the coolant exit was assumed equal to $\overline{u^2}/\alpha_1$ (see appendix). A turbulence intensity of 0.07 (from the experimental measurements) was used to compute this $\overline{u^2}$. The ratio of the turbulent kinetic energy to its rate of dissipation at $y=0$ was also estimated by $k/\epsilon = 1/(0.3\ \partial\overline{U}/\partial y)$.

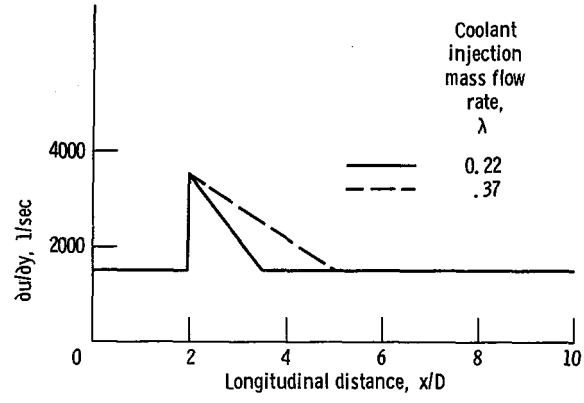

Figure 13. - Assumptions of $\partial\overline{U}/\partial y$ in $z = 0$ plane for numerical computation.

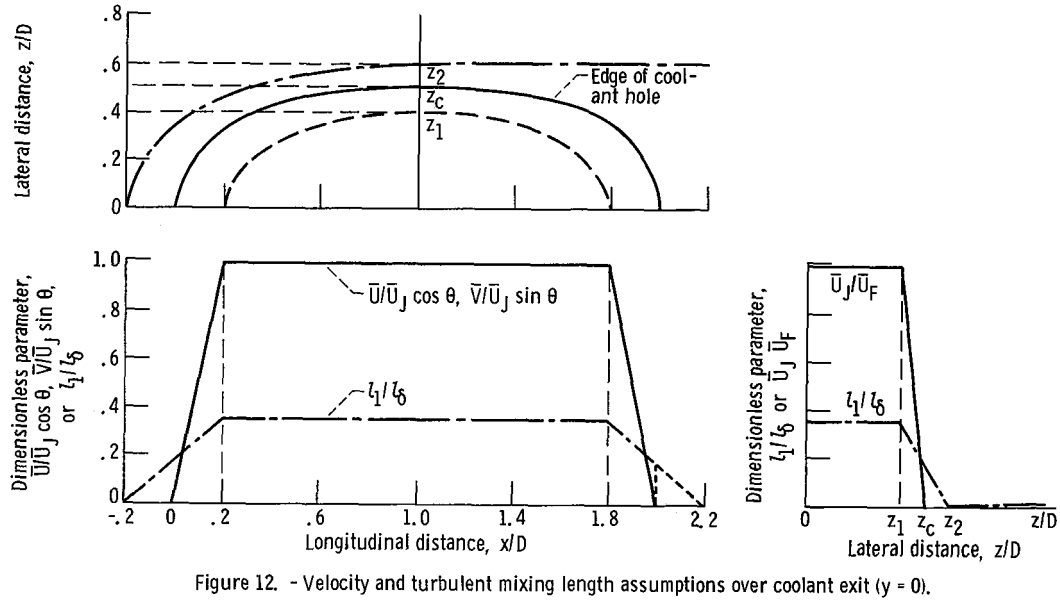

Figure 12. - Velocity and turbulent mixing length assumptions over coolant exit (y = 0).

Results and Discussion

To verify the effectiveness of the present turbulent mixing length models, some numerical results are presented and compared with experiments.

The Longitudinal Velocity Component

The numerical results of this velocity component are plotted in figures 14 to 16 for $\lambda = 0.22$ and 0.37. The present measurements are also shown in these figures for comparison.

For $\lambda = 0.22$ (figs. 14 and 15) a small $\overline{U}$ component was computed near the coolant exit. Good agreement between numerical prediction and experimental results is found after the coolant exit. But the numerical approach failed to predict the near-surface velocity at $z/D = 0.5$, the edge of the coolant hole (fig. 15). For large injection rates ($\lambda = 0.37$), good agreement between the numerical results and measurements within the symmetric plane is found only after the flow reattached to the surface (fig. 16).

The discrepency between the numerical results and measurements with large injection rate may be due to the simplicity of the present mixing length modeling. The linear distribution between two pivot points is not satisfactory near downstream edge of the coolant hole with $\lambda = 0.37$. Constants y_2 and l_2 might not be adequate to describe the mixing length distribution over the coolant exit region.

Analytically, the relation $k/\epsilon = 1/(0.3\ \partial\overline{U}/\partial y)$, which is valid within a local equilibrium turbulence boundary layer, was used as the boundary condition at $y = 0$. The velocity gradient was then computed with the law of the wall, assuming a laminar sublayer existed over the wall surface. For a large injection rate such as $\lambda = 0.37$, the $\overline{U}$ profile was significantly different from that in a flat plate turbulent boundary layer. This k/ϵ assumption might not be valid at high injection rate.

The normal velocity gradient was also imposed with a maximum value to eliminate the grid dimension effect in this study. To release this constraint, a large number of grid points should be used. Smaller step size in the x

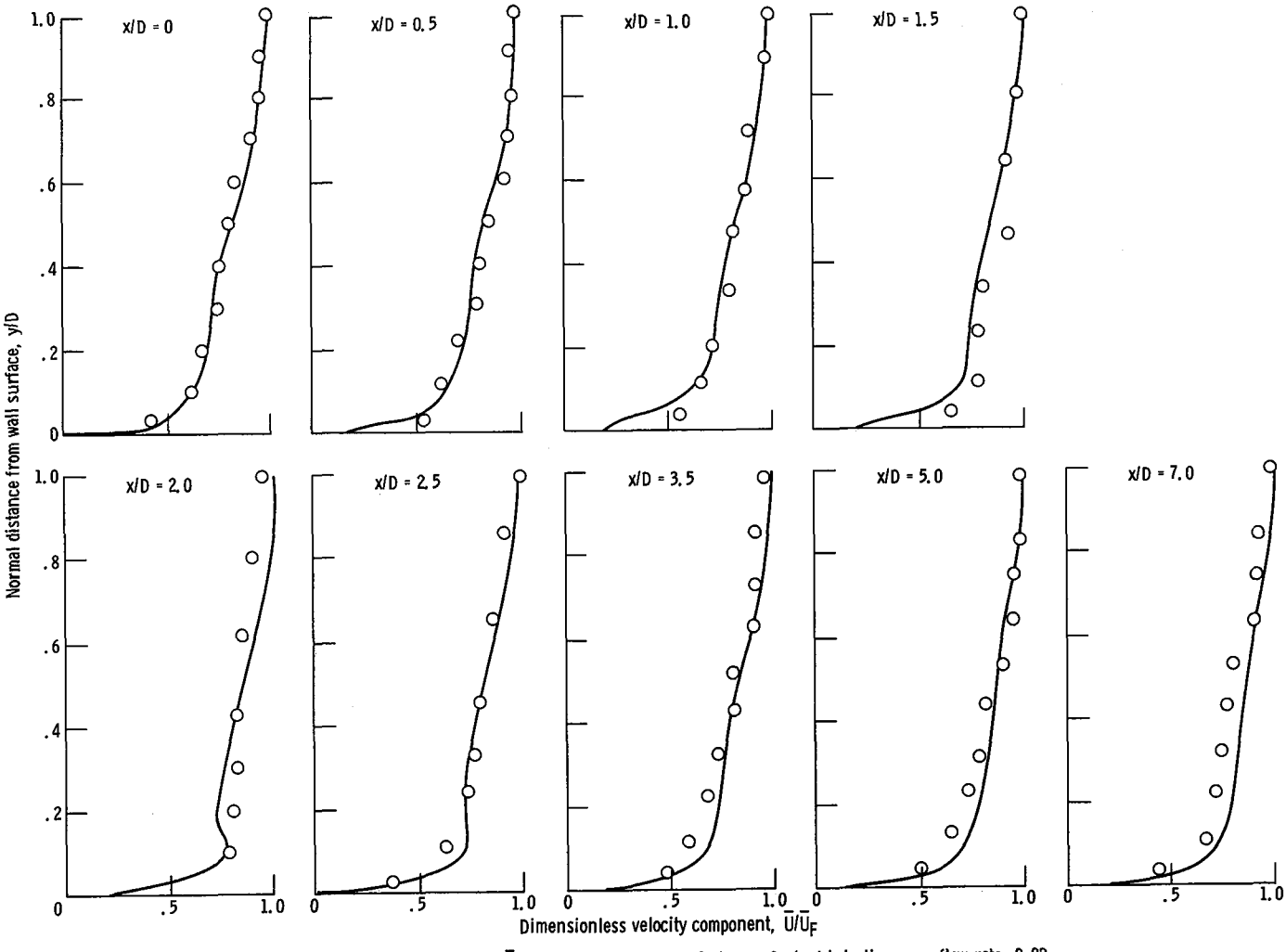

Figure 14. - Comparisons of $\bar{U}$ components in the z = 0 plane. Coolant injection mass flow rate, 0.22.

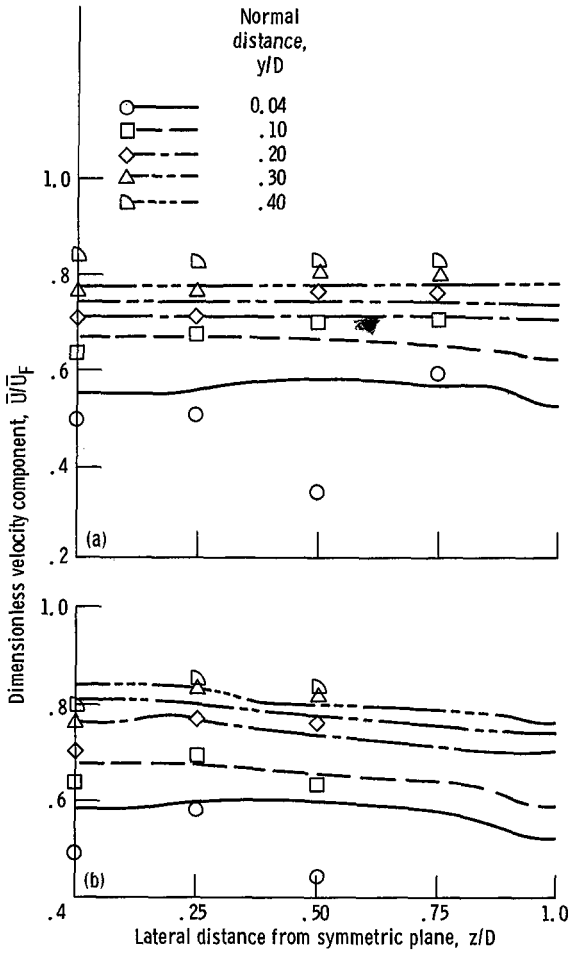

(a) Longitudinal distance, x/D = 3.5.
(b) Longitudinal distance, x/D = 5.0

Figure 15. - Comparisons of $\bar{U}$ component in lateral plane. Coolant injection mass flow rate, 0.22.

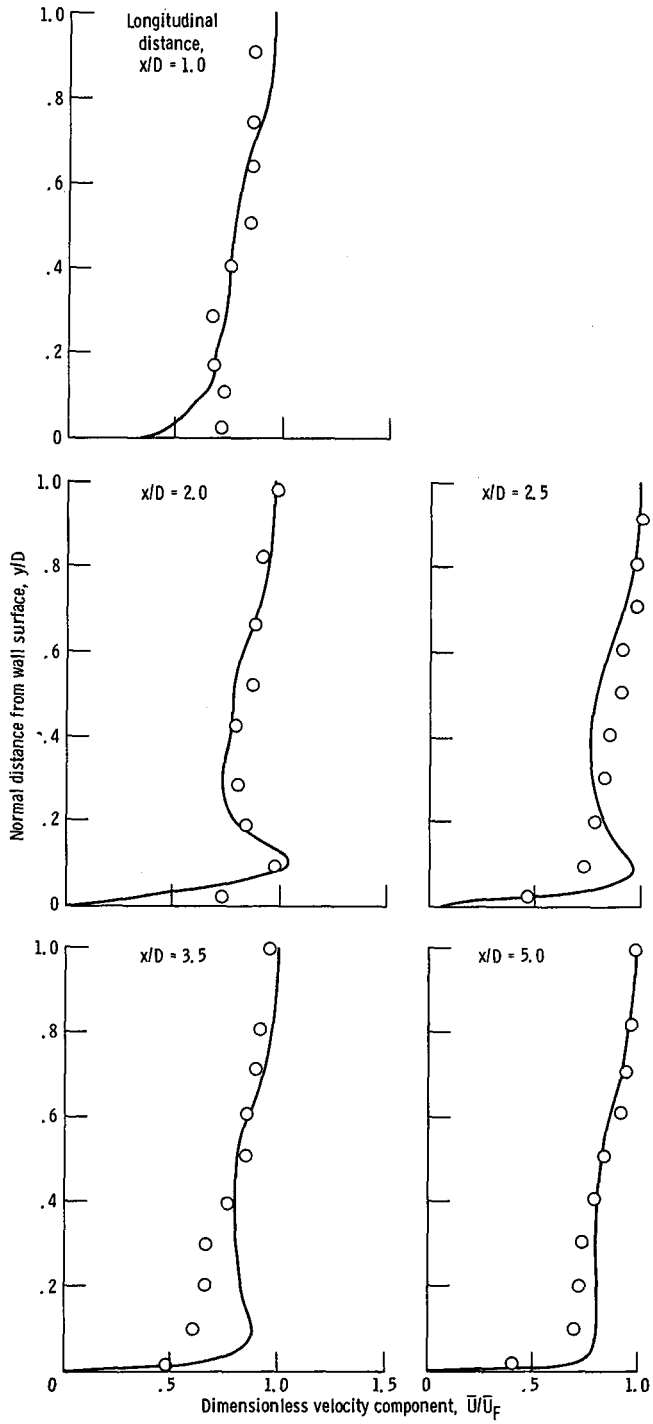

Figure 16. - Comparisons of $\bar{U}$ components in the z plane. Coolant injection mass flow rate, 0.37.

direction would also improve the numerical results, especially in the separated flow region. More extensive numerical computations might predict more accurately the properties in the near coolant hole flow field, especially for high coolant injection rate.

Surface Heat Transfer Rate

The numerical temperature profile was used to compute the local surface heat transfer rate. The second-order three-data-point-forward finite difference method was used to evaluate the temperature gradient at the wall surface. The local Stanton number then calculated

$$\mathrm{St} = k\frac{K(\partial T/\partial y)_{y=0}}{\rho_F \bar{U}_F C_P (T_F - T_w)}$$

From the initial profile $\mathrm{St}_0 = 0.0016$ was found. It is close to the value obtained from the flat plate boundary layer equation (ref. 12) with the present crossflow conditions ($T_F = 300$ K, $T_w = 278$ K, $\bar{U}_F = 22.9$ m/sec, and $R_F = 1.54 \times 10^6$).

The computational results of surface heat transfer rates in the $z = 0$ plane with $\lambda = 0.22$ and 0.37 are shown in figure 17.

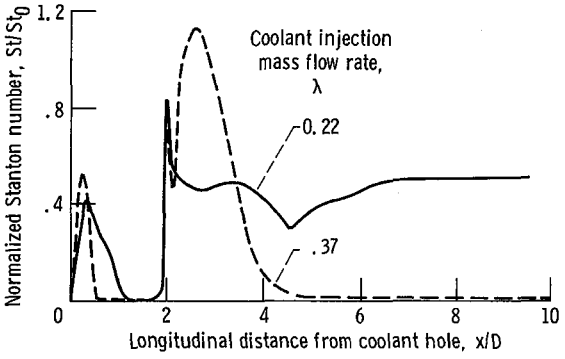

Figure 17. - Stanton number variations in z = 0 plane. Coolant to free-stream temperature ratio, T_j/T_F = 0.963; wall surface to free-stream temperature ratio, 0.926.

For $\lambda = 0.22$ significant reduction in the surface heat transfer rate downstream of the coolant hole was found. The maximum heat transfer rate was computed near the downstream edge of the coolant hole, and it reduced rapidly to a nearly constant value in the separated flow region. The surface heat transfer rate decreased again when the flow reattached to the wall surface and then increased to a constant value at locations far away from the coolant injection hole.

For $\lambda = 0.37$ a higher surface heat transfer rate (approximately the upstream undisturbed surface value) was computed immediately downstream of the coolant exit. This heat transfer rate reduced rapidly to a small value (nearly zero) after the flow reattached to the surface. A similar result has been measured from experiment (ref. 13). In many existing discrete-hole surface film cooling experiments, lower cooling effectiveness in the separated flow region with optimum cooling effectiveness in the reattachment flow region was reported at $\lambda \approx 0.4$. The difference between the present computational surface heat transfer rates along the plane of symmetry at $\lambda = 0.11$ and 0.37 is consistent with those experimental film cooling effectiveness.

The numerical results of the Stanton number in the lateral direction for $\lambda = 0.22$ are shown in figure 18. The Stanton number increases rapidly at $z/D \approx 1$ locations. The low surface heat transfer region ($St < St_0$) increased to twice the coolant hole diameter after the flow reattached to the surface. These phenomena are similar to the surface film cooling effectiveness described in references 3 and 9. A larger disturbed temperature field than the velocity field may occur at downstream locations. Using a small, constant y-z computational domain with the boundary conditions given at $z/D = 1$ (in the present computation) may induce the large lateral temperature gradient near $z/D = 1$. Using a large computational domain may reduce this lateral temperature gradient near the edge of the domain and provide higher computational surface heat transfer rates.

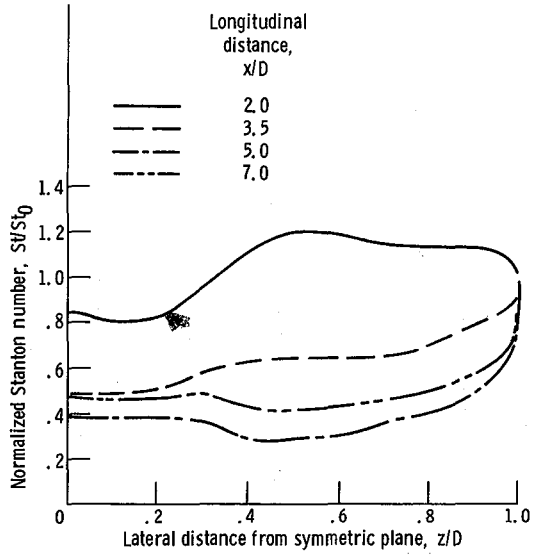

Figure 18. - Stanton number variations in lateral direction. Coolant injection mass flow rate, 0.22; coolant to free-stream temperature ratio, T_j/T_F, 0.963; wall surface to free-stream temperature ratio, T_W/T_F, 0.926.

Concluding Remarks

Three-dimensional mixing length models have been developed from the measurements of turbulence intensities within the flow field in a small region downstream of the discrete hole coolant injection at a 30° angle into a crossflow. Applying these models to a simplified three-dimensional theoretical and numerical analysis, the analysis predicted the longitudinal velocity distribution within the flow field with small coolant injection rates. With constant wall temperature, the numerical results showed a large reduction in the surface heat transfer rate downstream of the coolant hole. The distributions of the surface heat transfer rate were also consistant with the results of existing surface film cooling effectiveness studies.

The results of the present study also indicate that, with the aid of the mixing length models, existing three-dimensional flow field theory may provide a method of computing the surface heat transfer rate resulting from discrete-hole film cooling, including the effects of turbulence and the temperature of the coolant.

These mixing length models can be further improved with more elaborate experiments using a multiple, hot-wire sensor probe to measure the properties within the three-dimensional flow field. These additional data are necessary to completely define the mixing length models proposed here and to investigate the accuracy of the closure assumptions in the present analysis.

Lewis Research Center
National Aeronautics and Space Administration
Cleveland, Ohio, March 14, 1983

Appendix—Conservation Equations

The Cartesian directions x, y, and z were alined with the crossflow streamwise, vertical, and lateral directions, respectively, and the corresponding mean velocity components were designated $\overline{U}$, $\overline{V}$, and $\overline{W}$. The continuity, momentum, and enthalpy equations describing a steady, three-dimensional turbulent flow took the following forms, where, as discussed in the Theoretical Analysis of the Flow Field Section, the x-direction gradients of stresses and enthalpy flux and all pressure gradient terms were neglected.

$$\frac{\partial}{\partial x}(\rho\overline{U})+\frac{\partial}{\partial y}(\rho\overline{V})+\frac{\partial}{\partial z}(\rho\overline{W})=0 \tag{A1}$$

$$\frac{\partial}{\partial x}(\rho\overline{U^2})+\frac{\partial}{\partial y}(\rho\overline{VU})+\frac{\partial}{\partial z}(\rho\overline{WU})$$

$$=\frac{\partial}{\partial y}\left(\mu\frac{\partial\overline{U}}{\partial y}-\rho\overline{uv}\right)+\frac{\partial}{\partial z}\left(\mu\frac{\partial\overline{U}}{\partial z}-\rho\overline{uw}\right) \tag{A2}$$

$$\frac{\partial}{\partial x}(\rho\overline{UV})+\frac{\partial}{\partial y}(\rho\overline{V^2})+\frac{\partial}{\partial z}(\rho\overline{WV})$$

$$=\frac{\partial}{\partial y}\left(2\mu\frac{\partial\overline{V}}{\partial y}-\rho\overline{v^2}\right)+\frac{\partial}{\partial z}\left[\mu\left(\frac{\partial\overline{V}}{\partial z}+\frac{\partial\overline{W}}{\partial y}\right)\right] \tag{A3}$$

$$\frac{\partial}{\partial x}(\rho\overline{UW})+\frac{\partial}{\partial y}(\rho\overline{VW})+\frac{\partial}{\partial z}(\rho\overline{W^2})$$

$$=\frac{\partial}{\partial y}\left[\mu\left(\frac{\partial\overline{W}}{\partial y}+\frac{\partial\overline{V}}{\partial z}\right]\right)+\frac{\partial}{\partial z}\left(2\mu\frac{\partial\overline{W}}{\partial z}-\rho\overline{w^2}\right) \tag{A4}$$

and

$$\frac{\partial}{\partial x}(\rho\overline{UT})+\frac{\partial}{\partial y}(\rho\overline{VT})+\frac{\partial}{\partial z}(\rho\overline{WT})$$

$$=\frac{\partial}{\partial y}\left(\frac{K}{C_p}\frac{\partial T}{\partial y}-\rho\overline{vt}\right)+\frac{\partial}{\partial z}\left(\frac{K}{C_p}\frac{\partial T}{\partial z}-\rho\overline{wt}\right) \tag{A5}$$

Boundary Conditions

For the numerical solution of equations (A1) to (A5), the upstream undistributed two-dimensional mean velocity and mean temperature profiles must be specified. These profiles could be supplied by either assumption or measurement. For the present study the mean velocity profile was measured, and the mean temperature profile was computed using

$$\frac{T-T_w}{T_F-T_w}=\frac{\overline{U}}{\overline{U}_F} \tag{A6}$$

The following table lists other necessary boundary conditions:

Boundary	y/D	U	V	W	T
Wall surface	0	0	0	0	T_w
Coolant exit	0	$\overline{U}_j\cos\theta$	$\overline{U}_j\sin\theta$	0	T_J
Top surface (free stream)	∞	$\overline{U}_F$	0	0	T_F
Symmetric place ($z=0$)	y/D	$\partial\overline{V}/\partial z=0$	$\partial\overline{V}/\partial z=0$	0	---
z, $x\leq 0$	y/D	Initial profile	0	0	Eq. (A6)

Since the present study was directed at a small region near the coolant exit, the tube wall effect on the velocity distribution at the coolant exit ($0\leq x/D\leq 2$ and $y/D=0$) was included. However, uniform coolant temperature was used.

Closure Assumptions

To solve the governing equations with the specified boundary conditions, the constitutive equations for the turbulence terms are required for the momentum and enthalpy equations. For the present study the following Reynolds stress transport equations developed for the thin shear flow analysis (ref. 14) are used in the momentum equations ((A2) to (A4)).

$$\overline{u^2}=\frac{\alpha_1}{\alpha_2}l^2\left[\left(\frac{\partial\overline{U}}{\partial y}\right)^2+\left(\frac{\partial\overline{U}}{\partial z}\right)^2\right] \tag{A7}$$

$$\overline{v^2}=\frac{2F_{12}+\alpha_1-2}{\alpha_2}l^2\left(\frac{\partial\overline{U}}{\partial y}\right)^2$$

$$+\frac{F_{12}}{\alpha_2}l^2\left[\left(\frac{\partial\overline{U}}{\partial y}\right)^2+\left(\frac{\partial\overline{U}}{\partial z}\right)^2\right] \tag{A8}$$

$$\overline{w^2} = \frac{2F_{12}+\alpha_1-2}{\alpha_2} l^2 \left(\frac{\partial \overline{U}}{\partial z}\right)^2 + \frac{F_{12}}{\alpha_2} l^2 \left[\left(\frac{\partial \overline{U}}{\partial y}\right)^2 + \left(\frac{\partial \overline{U}}{\partial z}\right)^2\right] \quad \text{(A9)}$$

$$\overline{uv} = -l^2 \frac{\partial \overline{U}}{\partial y}\left[\left(\frac{\partial \overline{U}}{\partial y}\right)^2 + \left(\frac{\partial \overline{U}}{\partial z}\right)^2\right]^{1/2} \quad \text{(A10)}$$

$$\overline{uw} = -l^2 \frac{\partial \overline{U}}{\partial z}\left[\left(\frac{\partial \overline{U}}{\partial y}\right)^2 + \left(\frac{\partial \overline{U}}{\partial z}\right)^2\right]^{1/2} \quad \text{(A11)}$$

where $\alpha_1 = \overline{u^2}/k$, $\alpha_2 = (\overline{uv}^2 + \overline{uw}^2)^{1/2}$, and $F_{12} = F_{12}(\alpha_1, \alpha_2)$.

A set of the values, $\alpha_1 = 0.94$, $\alpha_2 = 0.26$, and $F_{12} = 0.59$, which are applicable to 90° corner boundary layer flow within a rectangular duct of arbitrary aspect ratio, has been established from experiment (ref. 14). These constant values are used here to correlate the present crossflow streamline $\overline{u^2}$ measurements. The y-direction distribution of the local mixing length, as it is computed from equation (A7), can be approximated with segments of linear y function. The experimental local mixing length is used to evaluate $\overline{u^2}$, $\overline{w^2}$, $\overline{uv}$, and $\overline{uw}$ terms in the momentum equations.

The heat-transfer counterparts

$$\overline{vt} = -\frac{1}{3.2}\frac{k}{\epsilon}\overline{v^2}\frac{\partial \overline{T}}{\partial y} \quad \text{(A12)}$$

$$\overline{wt} = -\frac{1}{3.2}\frac{k}{\epsilon}\overline{w^2}\frac{\partial \overline{T}}{\partial z} \quad \text{(A13)}$$

(from ref. 5) are assumed in equation (A5).

To find the rate of dissipation, the following transport equation was used:

$$\rho \overline{U}\frac{\partial \epsilon}{\partial x} + \rho \overline{V}\frac{\partial \epsilon}{\partial y} + \rho \overline{W}\frac{\partial \epsilon}{\partial z} = \frac{\partial}{\partial y}\left[\left(\mu + \frac{0.07\,\rho k^2}{\epsilon}\right)\frac{\partial \epsilon}{\partial y}\right] + \frac{\partial}{\partial z}\left[\left(\mu + \frac{0.07\,\rho k^2}{\epsilon}\right)\frac{\partial \epsilon}{\partial z}\right] + 1.44\,\rho \frac{P\epsilon}{k} - 1.9\frac{\rho \epsilon^2}{k} \quad \text{(A14)}$$

with the local generation rate

$$P = -\overline{uv}\frac{\partial \overline{U}}{\partial y} - \overline{uw}\frac{\partial \overline{U}}{\partial z} - \overline{v^2}\frac{\partial \overline{V}}{\partial y} - \overline{w^2}\frac{\partial \overline{W}}{\partial z} \quad \text{(A15)}$$

The ϵ profile at the edges of the domain of interest was evaluated with the boundary layer assumptions,

$$\epsilon = 0.3\,k\,(\partial \overline{U}/\partial Y)$$

Near the wall surface,

$$\epsilon = 0.09^{0.75}\,k^{1.5}/0.41/y$$

(ref. 5), was used. The boundary conditions at $y = 0$ (the wall surface) are $\epsilon = 0$ and $k/\epsilon =$ constant and at $y \approx \infty$ are $\epsilon = \epsilon_F$ and $\partial \epsilon/\partial y = 0$.

The corresponding boundary conditions at the coolant exit are given in the Numerical Method and Assumptions section.

References

1. Colladay, R. S.; Russell, L. M.; and Lane, J. M.: Streakline Flow Visualization of Discrete Hole Film Cooling with Holes Inclined 30° to Surface. NASA TN D-8175, Mar. 1976.
2. Jabbari, M. Y.; and Goldstein, R. J.: Effect of Mainstream Acceleration on Adiabatic Wall Temperature and Heat Transfer Downstream of Gas Injection. International Heat Transfer Conference, 6th vol. 5. Hemisphere Publishing Corp., 1978, pp. 249-254.
3. Papell, S. S.; Graham, R. W.; and Cageoa, R. P.: Influence of Coolant Tube Curvature on Film Cooling Effectiveness as Detected by Infrared Imaginery. NASA TP-1546, Nov. 1979.
4. Bergeles, G.; Gosman, A. D.; and Launder, B. E.: The Prediction of Three-Dimensional Discrete-Hole Cooling Processes, Part 1: Laminar Flow. J. Heat Transfer, vol. 98, no. 3, Aug. 1976, pp. 379-394.
5. Bergeles, G.; Gosman, A. D.; and Launder, B. E.: The Turbulent Jet in a Cross Stream at Low Injection Rates: A Three-Dimensional Numerical Treatment. Numer. Heat Transfer, vol. 1, Apr.-June 1978, pp. 217-242.
6. Bergeles, G.; Gosman, A. D.; and Launder, B. E.: The Prediction of Three-Dimensional Discrete Hole Cooling Processes, Part 2: Turbulent Flow. J. Heat Transfer, vol. 103, no. 1, 1981, pp. 141-145.
7. Patankar, S. V.; and Spalding, D. B.: A Calculation Procedure for Heat, Mass, and Momentum Transfer in Three-Dimensional Parabolic Flows. Int. J. Heat Mass Transfer, vol. 15, Oct. 1972, pp. 1787-1806.
8. Cary, A. M., Jr.; Bushnell, D. M.; and Hefner, J. N.: Predicted Effects of Tangential Slot Injection on Turbulent Boundary Layer Flow Over a Wide Speed Range. J. Heat Transfer, vol. 101, no. 4, Nov. 1979, pp. 699-704.
9. Papell, S. S.; Wang, C. R.; and Graham, R. W.: Film-Cooling Effectiveness with Developing Coolant Flow Through Straight and Curved Tubular Passages. NASA TP-2062, Nov. 1982.
10. Hanjalic, K.; and Launder, B. E.: A Reynolds Stress Model of Turbulence and Its Application to Thin Shear Flow. J. Fluid Mech., vol. 52, pt. 4, 1972, pp. 609-638.
11. Patankar, S. V.; and Spalding, D. B.: Heat and Mass Transfer in Boundary Layer. CRC Press, 1967.
12. Schlichting, H.: Boundary Layer Theory. Fourth ed., McGraw-Hill Book Company, Inc., 1960.
13. Loftus, P. J.; and Jones, T. V.: The Effect of Temperature Ratios on the Film Cooling Process. ASME Paper 82-GT-305, Apr. 1982.
14. Gessner, F. B.; and Emery, A. F.: A Length-Scale Model for Developing Turbulent Flow in Rectangular Duct. J. Fluids Eng., vol. 99, no. 2, June 1977, pp. 347-356.

1. Report No.	2. Government Accession No.	3. Recipient's Catalog No.
NASA TP-2200		

4. Title and Subtitle	5. Report Date
THREE-DIMENSIONAL TURBULENT-MIXING-LENGTH MODELING FOR DISCRETE-HOLE COOLANT INJECTION INTO A CROSSFLOW	September 1983
	6. Performing Organization Code 505-31-42

7. Author(s)	8. Performing Organization Report No.
Chi-Rong Wang and S. Stephen Papell	E-1497
	10. Work Unit No.

9. Performing Organization Name and Address	11. Contract or Grant No.
National Aeronautics and Space Administration Lewis Research Center Cleveland, Ohio 44135	
	13. Type of Report and Period Covered Technical Paper

12. Sponsoring Agency Name and Address	14. Sponsoring Agency Code
National Aeronautics and Space Administration Washington, D. C. 20546	

15. Supplementary Notes

16. Abstract

Three-dimensional mixing length models of a flow field immediately downstream of coolant injection through a discrete circular hole at a 30° angle into a crossflow were derived from the measurements of turbulence intensity. To verify their effectiveness, the models were used to estimate the anisotropic turbulent effects in a simplified theoretical and numerical analysis to compute the velocity and temperature fields. With small coolant injection mass flow rate and constant surface temperature, numerical results of the local crossflow streamwise velocity component and surface heat transfer rate are consistent with the velocity measurement and the surface film cooling effectiveness distributions reported in previous studies.

17. Key Words (Suggested by Author(s))	18. Distribution Statement
Film cooling Boundary layer flow Turbulence	Unclassified - unlimited STAR Category 34

19. Security Classif. (of this report)	20. Security Classif. (of this page)	21. No. of Pages	22. Price*
Unclassified	Unclassified	15	A02

* For sale by the National Technical Information Service, Springfield, Virginia 22161 NASA-Langley, 1983